ACS APPLIED MATERIALS & INTERFACES

Research Article

www.acsami.org

Asymmetric Reduction of Gold Nanoparticles into Thermoplasmonic Polydimethylsiloxane Thin Films

Jeremy R. Dunklin,[†] Gregory T. Forcherio,[‡] Keith R. Berry, Jr.,[†] and D. Keith Roper*[,†,‡]

[†]Ralph E. Martin Department of Chemical Engineering, University of Arkansas, Fayetteville, Arkansas 72701, United States

[‡]MicroElectronics-Photonics Program, University of Arkansas, Fayetteville, Arkansas 72701, United States

ABSTRACT: Polymer thin films containing gold nanoparticles (AuNPs) are of growing interest in photovoltaics, biomedicine, optics, and nanoelectromechanical systems (NEMs). This work has identified conditions to rapidly reduce aqueous hydrogen tetrachloroaurate (TCA) that is diffusing into one exposed interface of a partially cured polydimethylsiloxane (PDMS) thin film into AuNPs. Nanospheroids, irregular gold (Au) networks, and micrometer-sized Au conglomerates were formed in a ∼5 μm layer at dissolved TCA contents of 0.005, 0.05, and 0.5 mass percent, respectively. Multiscale morphological, optical, and thermal properties of the resulting asymmetric AuNP-PDMS thin films were characterized. Reduction of TCA diffusing into the interface of partially cured PDMS film increased AuNP content, robustness, and scalability relative to laminar preparation of asymmetric AuNP-PDMS thin films. Optical attenuation and thermoplasmonic film temperature due to incident resonant irradiation increased in linear proportion to the order of magnitude increases in TCA content, from 0.005 to 0.05 to 0.5 mass percent. At the highest TCA content (0.05 mass percent), an asymmetric PDMS film 52-μm-thick with a 7 μm AuNP-containing layer was produced. It attenuated 85% of 18 mW of incident radiation and raised the local temperature to 54.5 °C above ambient. This represented an increase of 3 to 230-fold in photon-to-heat efficiency over previous thermoplasmonic AuNP-containing systems.

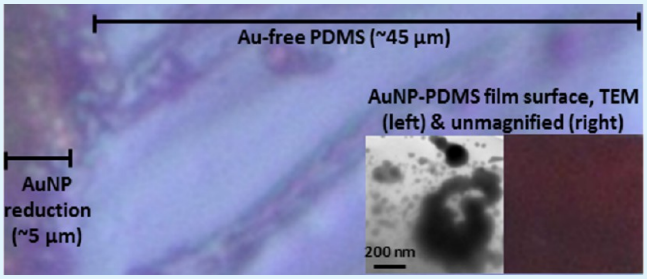

KEYWORDS: *nanocomposites, plasmonic heating, polymer films, nanoparticle interfaces, metamaterials*

1. INTRODUCTION

The optical and thermal properties of polymer nanocomposite films consisting of gold nanoparticles (AuNPs) have received increased interest in a variety of applications. Resonant irradiation of AuNPs deposited in polymer films allows precise, localized control of optical and thermal energy for photovoltaics,[1−4] sensing,[5−9] optoelectronic devices,[10−15] and catalytic reactions.[16,17] AuNPs formed in microporous cellulose acetate membranes and polydimethylsiloxane (PDMS) gels and foams have been shown to enhance solvent flux as well as remove aromatic solvents and sulfur contaminants from water, respectively.[18,19] Dense nonporous polymer films featuring randomly dispersed AuNPs have been formed by *in situ* reduction of dissolved gold salt and by mixing of gold into the polymer prior to curing.[20−22] However, thin films with AuNPs at just one interface could offer improved economics and operational benefits such as higher solvent flux and lower bulk membrane disruption in separations. While optical and thermal properties have been described for PDMS films featuring uniformly dispersed AuNPs,[22] these properties of asymmetric AuNP-PDMS films remain largely uncharacterized.

This work identified conditions to rapidly reduce AuNPs into a partially-cured PDMS thin film at a single interface by introducing hydrogen tetrachloroaurate ($HAuCl_4$, TCA) solution via solution diffusion. Effects of TCA concentration over a two-log range were examined. Two key benefits of asymmetric AuNP-PDMS thin films relative to films in which AuNPs were dispersed throughout were superior photon-to-heat conversion and scalability of AuNP deposition. Zhang et al. first fabricated asymmetric AuNP-PDMS films by exposing fully-cured PDMS films to TCA for up to one week at constant TCA concentration and variable cross-linker ratio.[23] The present work showed that partial curing of PDMS film allowed reduction of dilute, aqueous TCA into AuNPs within 24 hours via solution diffusion into an exposed film interface. Adjusting the dilution concentration, pre-cure time, and diffusion time influenced the resulting penetration depth, Au structure morphology, optical properties, and thermal properties. An alternative approach was examined in which a thin (∼25 μm) TCA-containing PDMS superstrate was spin coated onto a thicker, Au-free PDMS substrate. This latter approach produced asymmetric AuNP-PDMS films at a narrower range of comparable optical properties, but with inferior physical properties and scalability.

Incorporating nanoparticles into polymer films has been of significant recent interest. For example, Shi et al. demonstrated a method to print patterned gold film onto a PDMS-based dielectric layer in organic thin-film transistors by utilizing the *in*

Received: May 17, 2013
Accepted: August 9, 2013
Published: August 9, 2013

   dx.doi.org/10.1021/am4018785 | *ACS Appl. Mater. Interfaces* 2013, 5, 8457−8466

situ PDMS cross-linking process and analyzed the resulting electrical and surface properties.[11] AuNPs incorporated into the active layer of polymer solar cells were recently shown to enhance light absorption.[2] Organic gels doped with dispersed gold nanoparticles were studied for improved catalytic activity.[17] Recently, the effects of nanoparticle shape and concentration on the resulting thermophysical properties of nanoparticle-polymer systems were also examined.[24] Nergiz et al. demonstrated that the manipulation of pH allowed the tuning of structure and plasmonic properties of gold nanoparticles absorbed on an ultrathin polymer film.[6] Increased charge transfer via improved nanoparticle dispersion and the resulting spatiotemporal structure of semiconducting nanoparticle-polymer blends were recently investigated.[10] These reports characterize a range of physical, electrical, and spectroscopic properties of polymer nanocomposites that incorporate nanoparticles either on the surface or distributed throughout. This work extends this range to include fabrication and characterization of AuNP-containing asymmetric thin films and shows important advantages relative to uniformly distributed particles via sub-surface introduction of AuNPs at just one interface of a polymer.

Characterization of multiscale morphological, optical, and thermoplasmonic properties of the asymmetric AuNP-PDMS thin films showed significant effects as TCA concentration increased. An asymmetric gold layer was formed in a ∼50-μm-thick PDMS film at TCA contents ranging from 0.5 to 0.005 mass percent as aqueous TCA was solubilized by, and diffused into, one exposed interface of partially-cured PDMS thin film. Optical and electron microscopy showed that increasing TCA concentration substantially changed polymer structure and nanoparticle morphologies as well as interfacial thickness in the AuNP-containing layer of the asymmetric AuNP-PDMS thin films. At 0.005 mass percent TCA, dispersed particles were embedded to a depth of about 3 μm in a planar PDMS surface. At 0.05 mass percent, irregular Au networks appeared distributed to a depth of about 3 μm throughout an undulating PDMS surface. At 0.5 mass percent, densely packed nanoparticles appeared to a depth of 7 μm on a cratered PDMS surface. However, most AuNPs observable by TEM were nanospheroids $\leq$ 20 nm, despite these other microscopic morphological changes in polymer and Au structures. This resulted in a spectral feature with relatively constant bandwidth and energy whose intensity increased with TCA content.

Temperature increases in diffusive and laminar asymmetric films were induced by laser excitation near the localized surface plasmon resonance (LSPR) of AuNPs. A photon-to-heat conversion of up to 3000 °C/watt was demonstrated in the diffusive films, which represented a 3−230× increase over previous AuNP-functionalized systems. Optical attenuation and temperature change increased in parallel with the $\log_{10}$ of TCA solution concentration. Optical and thermoplasmonic responses were examined with and without an adjacent mesh support, which increased attenuation but decreased thermal response. With these observations in mind, the potential for employing asymmetric AuNP-PDMS thin films in thermoplasmonic pervaporation was considered.

2. EXPERIMENTAL SECTION

2.1. Polymer Preparation. PDMS (Sylgard 184 silicone elastomer kit #4019862) was purchased from Dow Corning (Midland, MI, USA). Hydrogen tetrachloroaurate(III) (TCA; $HAuCl_4 \cdot 3H_20$, G4022) was purchased from Sigma-Aldrich (St. Louis, MO, USA). All processes were performed at ambient temperature and pressure, unless noted otherwise. A speed mixer (DAC 150SP, FlackTek, Inc., Landrum, SC, USA) was used to mix the PDMS and curing agent mixture at 3035 rpm for 4 minutes. The mixture was degassed for 20 minutes to ensure gas bubbles were not present within the mixture.

2.2. Diffusive Method. TCA solution obtained from the manufacturer was diluted with distilled, deionized (DD) water to 25 mass percent TCA. Mass percent was calculated as the mass of pure TCA relative to the mass of the entire dilute solution. This solution was diluted further with DD water to the desired TCA content. Au-free PDMS, made with a cross-linker to monomer ratio (η) of 0.10, was spin-coated on a 1 in. × 1 in. × 0.04 in. glass substrate at 1000 rpm for 90 s and then cured at room temperature for 24 h. Each PDMS film was approximately 0.03 g. This partially-cured PDMS thin film was exposed to TCA solutions from 0.005 mass percent (0.00015 M) to 0.5 mass percent (0.15 M) for 24 hours in a sample box (1 in. × 1 in. × 0.25 in.) wrapped in parafilm to prevent evaporation. Enough TCA solution (approximately 2 mL) was used to ensure that the PDMS surface was completely submerged in the TCA solution. The Au-reduced film was fully cured for 15 minutes on a hot plate at 180 °C. As a control, Au-free PDMS thin films were fabricated using the same approach, except DD water was used instead of the gold solution.

2.3. Laminar Method. This method produced asymmetric AuNP-PDMS thin films by sequentially spin-coating a Au-free PDMS solution followed by a TCA-containing PDMS mixture onto a glass substrate. The initial layer of Au-free PDMS was spin-coated on the substrate for 90 s at 1500 rpm, then cured at 180 °C for 10 min. A 1.2 mass percent TCA mixture was prepared by mixing 0.0223 g of 25 mass percent aqueous TCA and 0.4855 g of PDMS. This mixture was spin-coated on top of the Au-free PDMS film at 4000 rpm. The resulting mixture was a dark purple, indicating that significant AuNP reduction occurred during mixing. The laminate was then fully cured for 15 minutes on a hot plate at 180 °C, which provided cohesiveness between the two layers.

2.4. Sample Imaging. Surface and cross-sectional images were taken with a digital camera (Infinity 1-5, Lumenera Corporation, Ottawa, CA) integrated with a light microscope (Eclipse LV100, Nikon Instruments, Melville, NY, USA) in brightfield reflection mode. Cross-sectioning was performed by cutting small sections of the film, and placing it between two glass microscope slides. Dimensions within the thin films and asymmetric AuNP-containing layer were characterized using image analysis software (Infinity Analyze, Lumenera Corporation, Ottawa, CA). A digital camera was used to take the unmagnified images of the different thin films. Scanning electron microscopy (SEM) was performed using a Philips XL40 FEG. Transmission electron microscopy (TEM) was performed with a XFI Titan 80-300 HRTEM.

2.5. Optical Characterization. Fractional transmission and reflection of the thin films were measured at 532 nm with an apparatus recently described by Forcherio and Roper.[25] Each sample was affixed to the exterior of an integrating sphere (IS200-4, Thorlabs, Newton, NJ, USA) and irradiated at normal incidence from the opposite side of the sphere at approximately 18 mW with a 532 nm diode laser (MXL-H-532, CNI, Changchun, CN). Each sample was measured with the Au-free PDMS layer facing the laser. A power meter (PM100D, Thorlabs, Newton, NJ, USA) captured forward scattering (i.e. transmission), and a spectrometer (AvaSpec-2048, Avantes, Broomfield, CO, USA) detected reverse scattering (i.e. reflection) coupled by the integrating sphere. A spectrometer was used to measure scattered intensity because in practice its accuracy and reliability were superior to those of a power meter or silicon photodiode. Only intensity was reported because light was incident on the sample at a single wavelength (532 nm). Integration of a white light source into the integrating sphere system is the subject of ongoing work.

The difference between the sum of these fractions, transmission (T_i) and reflection (R_i), and unity (1) represents the fractional attenuation (A_i). Attenuation includes plasmonic absorption and bulk losses.

$$A_i = 1 - (T_i + R_i) \quad (1)$$

Three trials were conducted for each sample to capture any operational, measurement, and sample variability. The reported values for transmission and reflection reflect the average of these trials, and the uncertainty reflects the standard deviation from the mean. UV−vis absorbance spectra were taken with a spectrometer (Ocean Optics, USB-4000, Dunedin, FL, USA) and a deuterium-halogen light source (Avalight, DH-S-BAL, Avantes, Broomfield, CO, USA).

2.6. Thermal Data Collection. Thermal data were captured using 5 mm × 5 mm samples of the films suspended vertically with the laser spot (1.2 mm diameter) centered within the film. This method was similar to that used in a previous report.[22] The infrared thermal imaging camera (ICI 7320, Infrared Cameras Inc., Beaumont, TX, USA) was placed on the opposite side of the film and focused on the film for temperature data collection. The laser power was set to 18 mW to match both the power used in the integrating sphere setup and to keep the infrared camera within its operational temperature range (<100 °C). Laser power was monitored before and after each trial to make sure it did not vary significantly. The setup was enclosed in a plexiglass environmental chamber to eliminate forced convection. The infrared camera recorded the thermal data at 1 Hz during a 3 min heating period with the laser on and a 3 min cool down period with the laser turned off. The data were saved as images in which temperature values were recorded at each pixel in the image (320 × 240 pixels). These images were analyzed using Matlab R2012a (Mathworks, Natick, MA, USA) to produce the temperature distribution throughout the sample during irradiation.

3. RESULTS AND DISCUSSION

3.1. Diffusive Method for Asymmetric Thin Film Formation via TCA Reduction. This work identified a range of times and temperatures at which a partial cure of PDMS allowed rapid reduction of TCA at solution concentrations varying over two orders of magnitude. Previously, fabrication of asymmetric AuNP-PDMS films by exposing fully-cured PDMS film to TCA for up to one week had been reported.[23] At a constant 0.5% (m/v) TCA concentration, it had been shown that the spectral LSPR absorption, particle size, and penetration depth were a function of the curing agent to monomer ratio (η). Neither the penetration depth for each value of η nor its variation with exposure was precisely measured. However, it was reported that a large η value led to larger particles located almost exclusively on the surface of the polymer. The resulting composite films were shown to have potential in a variety of biochemical analyses on PDMS microchips.

The faster method developed and characterized in this work to form asymmetric AuNP-PDMS thin films was based on this and related prior work. It had been reported that η values greater than 0.10 should be used to keep the gold near the polymer surface.[23] However, using η values ranging from 0.15 to 0.20 in this work produced thin films prone to tearing. Durable thin films capable of repeated use are valued for scalable implementation. A related report indicated that the addition of $KAuCl_4$ resulted in brittle PDMS foams and gels,[19] further demonstrating the need for fabrication conditions that do not further compromise the structural integrity of the AuNP-PDMS thin films. A residual cross-linker in the body of the thin film at higher cross-linker concentrations could affect mass and thermal transport properties in the thin films, potentially complicating testing in applications. Therefore, the manufacturer's recommendation of η = 0.10 was used for all experiments herein to alleviate each of these concerns.

PDMS cross-linking occurs as a result of reaction between the monomer vinyl groups (Si−CH═CH_2) and the curing agent comprised of silicon hydroxide (Si−H) groups.[26] It has been proposed that $AuCl_4^-$ ions in the aqueous TCA solution diffuse into the PDMS matrix upon exposure.[23] These diffusing ions then react with the remaining Si−H groups, forming AuNPs. Partially cured PDMS differs from fully cured PDMS in that it contains a more available cross-linker (Si−H groups) able to further cross-link the monomer's vinyl groups. Ellipsometry measurements verified that residual Si−H concentration decreases at progressively longer curing times.[26] Partially cured PDMS is not visually distinct from fully cured PDMS: both are translucent and optically transparent (transmission of fully cured PDMS was ca. 90%). All samples were fully cured prior to any characterization. While higher temperatures are conventionally used to reduce curing time, there is no indication that changing curing temperature or time affects ultimate attainment of complete cross-linking. Curing at ambient temperature was adopted in this work to minimize macroscopic geometrical anisotropies in cross-linking caused by multidimensional conduction during partial cure on a hot plate or in a convection oven.

Partial curing yielded higher gold content when compared with the reduction of aqueous TCA diffusing into fully cured PDMS (15 min at 180 °C on a hot plate). These experiments, with 24−48 h TCA exposure times, led to pale pink films with too little gold for desirable optothermal response. Other combinations of time, temperature, and TCA content evaluated to speed TCA reduction via partial cure resulted in less optimal outcomes. Insufficient pre-cure (1−8 h under ambient conditions or 15 min at 50 °C on a hot plate) led to polymer degradation caused by the rapid consumption of cross-linker for gold reduction which resulted in some incurable films. Partial curing on either a hot plate or in an oven (80°C for 10 minutes) led to visible gold reduction similar to that observed via 24 h cure under ambient conditions, but only in the center of the sample.

The amount of gold that can be reduced in PDMS before the polymer loses its robustness has been reported to be limited to about 0.75 mass percent TCA (in PDMS) at η = 0.10.[27] Formation of an asymmetric AuNP-PDMS layer atop a Au-free PDMS substrate mitigates this limit to some extent. The film surface for the 0.5 mass percent sample remained slightly tacky for days, but the rest of the polymer cured fully, providing mechanical support to the more weakly cross-linked AuNP-containing layer. This contrast suggested residual monomer remained at the film surface, ostensibly due to rapid reduction of TCA into AuNPs, which left regions of the surface with no curing agent available to cross-link the remaining monomer. Thus, a concentration of 0.5 mass percent appeared to be the upper, functional limit for reduction of TCA diffusing into PDMS partially cured at ambient conditions for 24 h.

3.2. Laminar Method for Asymmetric Thin Film Formation via TCA Reduction. The laminar method resulted in practical limitations to AuNP-PDMS layer thickness, attainable optical properties, and scalability. This method produced a AuNP-containing layer thickness of about 25 μm at 4000 rpm, the highest possible speed allowable by the spin-coater that was used. The underlying Au-free PDMS layer was about 40 μm. Use of toluene has been reported to dilute the PDMS in order to spin-coat thinner layers at the same speed, but it is not anticipated that the thickness of the AuNP-PDMS layer would be less than 10−15 μm even with the toluene dilution.[28] Preliminary testing with toluene dilution of PDMS

that was greater than in the cited work led to negligible thickness reductions and inconsistent spin-coating.

3.3. Gold Formation Morphologies. Exposure of partially-cured PDMS film to solutions with increasing TCA content led to significant differences in the size, appearance, and density of Au nanostructures formed. TEM images for the 0.05 mass percent film are shown in Figure 1. A high number of

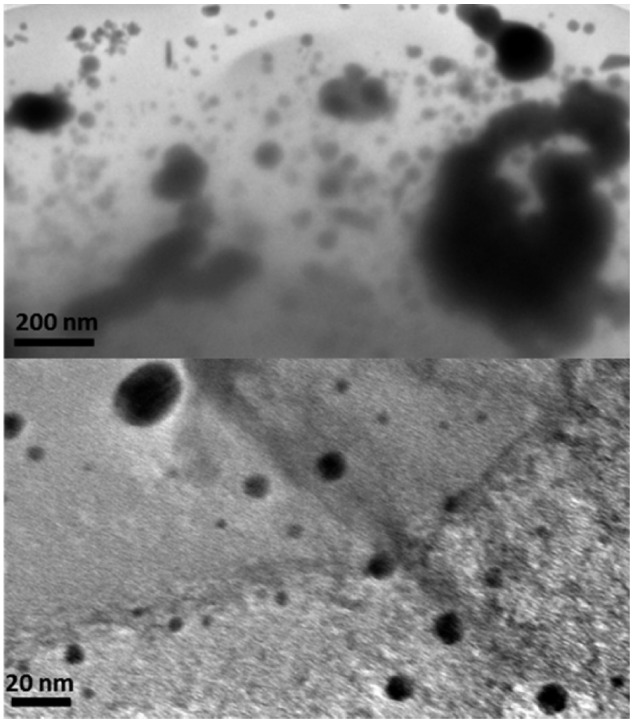

Figure 1. TEM images of 0.05 mass percent sample. Top picture shows large conglomerates visible in SEM images and AuNPs distributed throughout. Bottom picture shows AuNPs both on the polymer surface (top-left) and where the top surface has been removed (bottom-right).

randomly-distributed Au nanospheriods ≤ 20 nm are visible. In addition, large micrometer-scale Au conglomerates are visible at the polymer surfaces. These conglomerates were most common at 0.005 mass percent as shown in Figure 2, while at 0.5 mass percent the sample surface appeared composed almost entirely of densely-packed, sub-micrometer sized particles. Large gold structures formed on the 0.05 mass percent sample surface were comprised primarily of irregular tangled networks of gold. These structures are visible throughout the surface of the 0.05 mass percent SEM image and in its inset. These gold networks appeared in the 0.5 mass percent sample as well, but were less prevalent.

The relatively large Au conglomerates and tangled networks would not be expected to contribute to photon-to-heat conversion, although they would increase local thermal conductivity. Thermoplasmonic activity would arise from localized surface plasmon resonance induced by incident resonant irradiation on the ≤ 20 nm Au nanospheroids, whose signature dominates the spectral profile of each sample, particularly in the 0.5 mass percent sample in which conglomerates and irregular networks appear relatively scarce. This is explained more fully in section 3.7, Optical Characterization. Data obtained thus far suggest that large micrometer-sized particle conglomerates form less readily beneath the surface within the densely cross-linked PDMS, possibly precluded by the high volume fraction occupied by the existing polymer matrix.

Intense charging effects from PDMS hampered exhaustive characterization at 0.5 mass percent and precluded TEM of 0.5 and 0.005 mass percent films. The small surface area analyzed by TEM did not permit a rigorous analysis of size distribution for the entire film. However, previous work showed 13 nm mean diameter AuNPs formed at 0.5% (m/v) using the same $\eta = 0.10$.[23] The mean particle diameter of reduced AuNPs grew with increasing η, and the resulting particles became less spherical. Other methods to characterize AuNP size and distribution were hindered by the physiochemical stability of PDMS. These included dissolution in acids such as hot concentrated sulfuric acid. Mie theory approximations were used to attempt to ascertain size distribution but proved largely ineffective. Work is in progress to improve control and predictability of AuNP size and distribution during the fabrication process itself.

3.4. Film Appearance and Morphology. Microscopic images of the fabricated samples shown in Figure 2 indicate that film appearance and morphology evolved as TCA mass percent increased. However, the majority of AuNPs observable by TEM were ≤ 20 nm. These AuNP produced a localized surface plasmon (LSPR) spectral feature with relatively constant bandwidth and energy whose intensity increased as TCA content increased on a $\log_{10}$ scale, as shown in Figure 3. At the lowest TCA concentration, 0.005 mass percent, PDMS film appeared slightly less transparent than the Au-free PDMS thin film, with a slight pinkish tint. This was the only concentration of TCA that yielded an essentially optically transparent AuNP-PDMS film. Transparency is exhibited by the UV−vis absorbance spectra for the 0.005 mass percent film in Figure 3, which has a baseline extinction value similar to Au-free PDMS outside of the LSPR region near 532 nm. In contrast, the 0.5 and 0.05 mass percent extinction spectra exhibit significantly higher extinction values across the entire spectrum. As TCA concentration increased, the film hue deepened from a reddish-pink to a deep, opaque purple, indicative of more optically active AuNPs. Surfaces of the 0.05 and 0.5 mass percent samples were slightly reflective, even without magnification. Reflectivity appeared not to originate from gold film or bulk gold at the surface, but rather from changes in surface morphology occasioned by increasing Au content, as described next. Deepening hue and apparent reflectivity with increasing TCA content were similar to changes previously reported.[23]

SEM images in column 1 of Figure 2 show surface morphology of the AuNP-PDMS film evolved from planar to hilly to cratered as gold content increased from 0.005 to 0.05 to 0.5 mass percent, respectively. Craters are hypothesized to occur due to washout of uncured residual monomer following the 24 h ambient exposure period at higher TCA contents which consumed more cross-linker in partially-cured PDMS film. Degeneration of planar PDMS surface morphology at increased TCA content had not previously been reported. This suggests its origin may arise from the use of partial, rather than fully, cured PDMS. A possible benefit of surface cratering could be an increase in effective surface area of the thin film. This could enhance interfacial interactions such as pervaporation in future applications.

3.5. Nanoparticle Formation. The size and shape of surface gold structures reduced from TCA in the respective

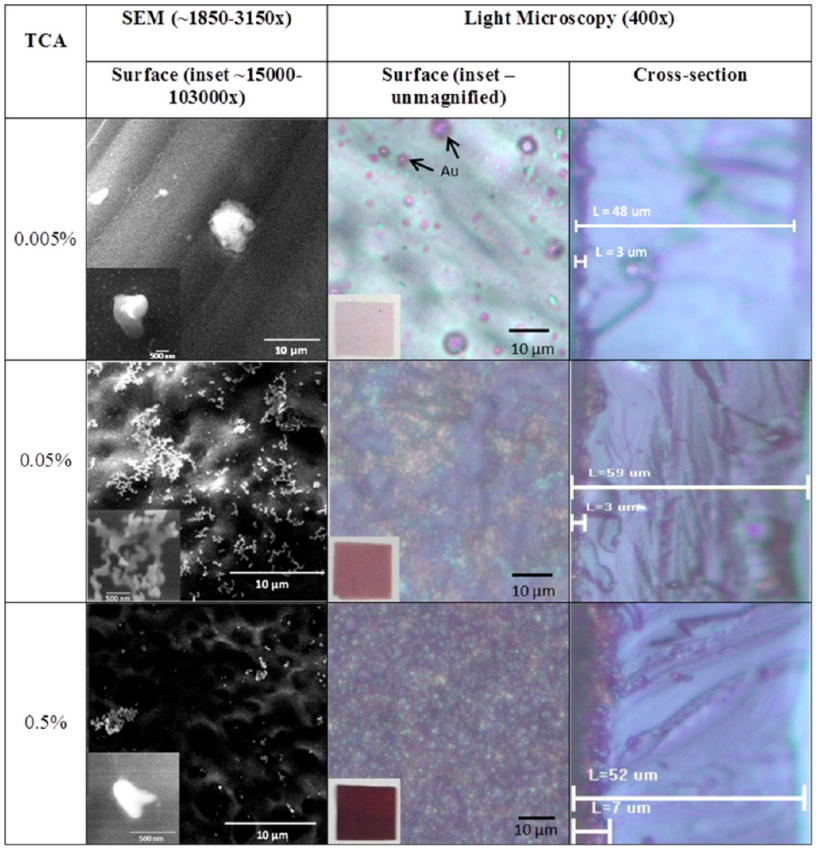

Figure 2. The differences in physical characteristics between the three different TCA dilution concentrations. Each row represents a single TCA concentration. The columns represent a single imaging method consistent across each sample with SEM surface images with an inset of a single large gold structure (left), optical microscopy surface images with an unmagnified inset (middle), and an optical microscopy cross-section displaying the approximate thicknesses of the Au-free PDMS and AuNP-containing containing layers.

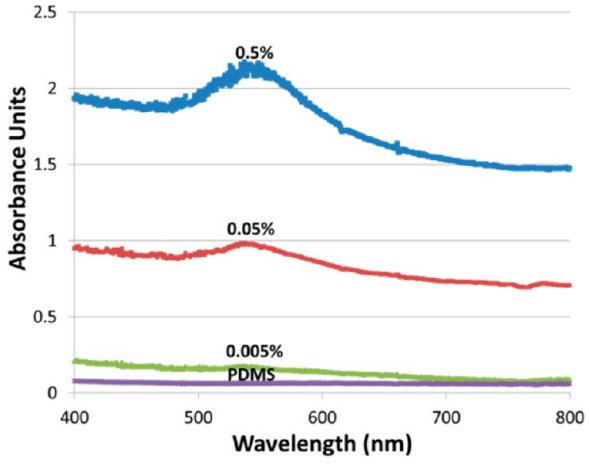

Figure 3. UV–vis absorbance spectra for the 0.5 mass percent (blue), 0.05 mass percent (red), and 0.005 mass percent (green) AuNP-PDMS films and Au-free PDMS. Absorbance peaks are at 532 nm, 535 nm, and 535 nm, for the 0.5, 0.05, and 0.005 mass percent samples, respectively.

samples resulted from an interplay between kinetics and thermodynamics of underlying nucleation and growth of existing structures. Respective rates of nucleation and growth determine particle size, morphology, and distribution. Nucleation results from molecules in solution first associating into a cluster (a small nanoparticle). This cluster may then dissociate or congeal and grow. At low concentrations, rapid nucleation coupled with growth can reduce the initial gold concentration past a critical point for new particle nucleation. At this point, growth and Ostwald ripening, the process where small particles redissolve in solution and attach to existing particles, become dominant. The appearance of micrometer-scale conglomerates could result from relative thermodynamic favorability of particle growth on the polymer surface at lower TCA concentrations. The exact causes of the irregular networks in the 0.05 mass percent in PDMS are unknown, but analogous structures were reported for calcium phosphate nanoparticles blended into a poly(3-hydroxybutyrate) (PHB) polymer.[24] It was reported that the polymer matrix structure influenced nanoparticle clustering and caused similar network formation on the nanoscale. Given the visible effects the reduction had on the surface, it is possible that the internal polymer structure was also affected, thus influencing subsequent nanoparticle formation.

Manipulation of nucleation and growth rates has been performed in order to control nanoparticle formations both in solution and in polymers. Homogenous growth of gold nanoparticles was performed by inhibiting secondary nucleation by adjusting temperature, TCA to seed particle concentration, and pH.[29] The rates of nucleation and growth of metallic nanoparticles formed via photoreduction were shown to be strongly affected by initial metal concentration.[30] Shape-controlled synthesis of hematite (iron) nanostructures was achieved by controlling the local iron ion availability for reaction with the use of different ligands, resulting in particles, rods, and chain structures similar to the networks seen here.[31]

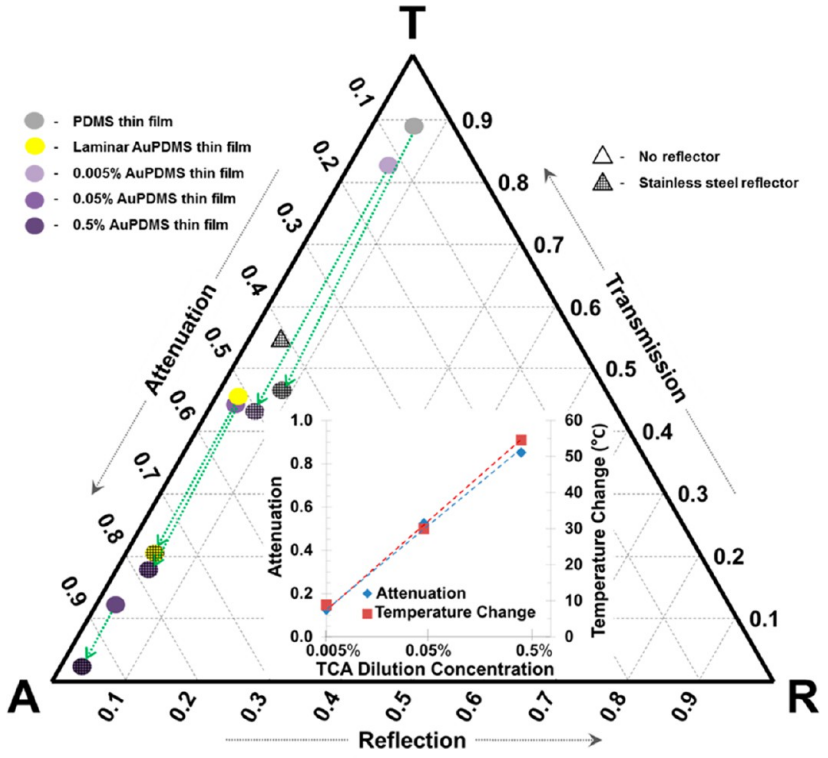

Figure 4. Measured fractional transmission (T), reflection (R), and attenuation (A) for AuNP-PDMS films with and without the support mesh. The triangle (△) represents the support mesh. Dotted green arrow lines represent the relative contribution of the support mesh by connecting each film with its corresponding data with the stainless steel mesh. The inset shows the linear relationship in the diffusive method between the $\log_{10}$ of TCA dilution concentration with attenuation and temperature change.

Increasing the ratio of reducing agent concentration relative to TCA concentration was shown to increase average particle size in the prior work utilizing diffusion of TCA into PDMS.[23] Exposure time was seen to have a strong effect on particle size in these prior investigations, but time was kept constant for all the samples in this work.

3.6. Characterization of Au Layer Formed via Diffusion. The measured AuNP penetration depths measured in microscopic cross-sections were orders of magnitude less than predicted by equations for unsteady diffusion at solid-liquid interfaces. This indicated the penetration depth was not controlled primarily by either aqueous or ionic gold diffusivities. Optical microscopy in the right-most column of Figure 2 shows that the thickness of the AuNP-containing layer is about 3 μm for both the 0.005 and the 0.05 sample and about 7 μm for the 0.5 mass percent. AuNP-containing layer thickness was greatest with the 0.5% sample, consistent with previous work indicating that the penetration depth of the gold nanoparticles increased as the ratio of cross-linker to TCA decreased.[23]

The penetration depth of reduced TCA into PDMS is about 0.001 of the diffusion depth expected for water into PDMS. Using a diffusivity of water in PDMS of approximately 2×10^{-9} m^2/s,[32] diffusive penetration of water into a semi-infinite PDMS slab would reach approximately 5 cm after 24 h. Penetration depth is defined as the point where the dimensionless concentration of water is 1% of that outside the PDMS. Diffusivities of various gold ionic species and AuNPs in aqueous media reportedly range from 10^{-9} to $10^{-11} m^2/s$.[33] Even at the lowest diffusivity of 10^{-11} m^2/s, the predicted penetration depth would be about 3 mm. This suggests TCA is largely reduced into nanostructures within the asymmetric AuNP-containing layer before further penetration via diffusion is possible. At the same time, reduction of AuNP at local sites is restricted by the availability of Si−H groups as well as TCA. Therefore, the penetration depth of AuNPs appears limited by a complex balance of thermodynamic driving force, local reduction potential, AuNP nucleation, and growth, rather than by diffusion alone. Development of a working description that would support predictable control of penetration depth within tens of nanometers is the subject of ongoing work.

3.7. Optical Characterization. UV−vis absorbance spectra for each sample are shown in Figure 3. Each spectrum exhibits a broad, localized surface plasmon resonance (LSPR) feature that peaks near 532 nm, the incident laser wavelength. The irregular networks, conglomerates, and microscopic particles appearing in Figure 2 minimally influence the peak wavelength of optical extinction. Specifically, LSPR features in Figure 3 spectra of the 0.5, 0.05, and 0.005 mass percent samples peaked at 532, 535, and 535 nm, respectively. The 3-nm redshift in the latter two samples would not significantly affect optothermal conversion at 532 nm, nor would it permit LSPR absorption at red or IR wavelengths to heat the system.

An integrating sphere was employed with a bi-directional spectroscopic apparatus to measure reflection and a power meter to simultaneously measure transmission of the asymmetric thin films. The film fabricated with a 0.5 mass percent TCA solution was observed to attenuate 0.8515 ± 0.0122 of normally incident resonant laser light. This represented a 70% improvement over a 130-μm-thick PDMS film with uniformly dispersed, reduced AuNPs from 0.6 mass percent TCA and 470% improvement compared to a 680 μm film consisting of 0.005 mass percent organic coated 16 nm AuNPs.[22,25] Attenuation for each diffusive thin film increased linearly in proportion to $\log_{10}$ increases in the initial TCA

Table 1. Photon-to-Heat Efficiency of Thermoplasmonic Nanocomposite Alternatives

physical description	system dimensions (mm)	gold content	laser power (W)	equilibrium ΔT (°C)	ΔT (°C) per watt
PDMS film in pervaporation system[27]	radius = 7.5, thickness = 0.135	0.6 mass percent TCA, reduced; uniformly dispersed	0.75	10	13.33
680 μm PDMS film in air[22]	5 × 5 × 0.68	0.1896 mass percent TCA, reduced; uniformly dispersed	0.1	72	720
fluid-filled AuNP-plated capillaries[34−36]	4 × 0.2 × 14	thermally annealed AuNP from EL gold film	0.1	26 (air)	260
				16 (butanol)	160
				14 (water)	140
AuNP colloidal solution in cell[36,37]	4 × 0.2 × 15.9	7.9 μL AuNP suspension of 920 g/m^3 in water	0.17	2.2	12.94
this study: 0.5 diffusive film	5 × 5 × 0.05	0.5 mass percent TCA, diffused	0.018	54.5	3028
this study: laminar film	5 × 5 × 0.065	1.2 mass percent TCA, reduced	0.018	28.2	1567

dilution concentration, as shown in the inset of Figure 4. The 0.05 and 0.005 mass percent samples attenuated 0.5241 ± 0.0122 and 0.1257 ± 0.0138 of incident irradiation, respectively, as illustrated in the triangular diagram of Figure 4. Attenuation of the laminar film was 0.5121 ± 0.0254, comparable to 0.05 mass percent. For comparison, the Au-free PDMS attenuated 0.0492 ± 0.0239. These results are consistent with the images of the film surfaces in Figure 2 that indicated the 0.005 mass percent film is highly transparent, while the higher concentrations have increased formation of optically active gold indicated by a deepening purple. Increasing TCA concentration in embedded films was previously shown to reduce the optothermal efficiency of the film on a per gold mass basis.[22] Determination of total gold content within the diffusive thin films in this work is the subject of future analysis of the diffusion reaction during reduction.

Measured fractional far-field transmission, reflection, and attenuation for individual components and paired systems are shown in the equilateral triangle diagram of Figure 4. Top, right, and left vertices in this figure correspond to unity (1) values of *T*, *R*, and *A*, respectively. Each point in the triangle represents a system with a unique, independent combination of measured *T* and *R*, and the related dependent value of *A*. Measured components and AuNP-PDMS/support mesh systems are distinguishable by color and shape and cross-hatch pattern (mesh support). Purple hues represent increasing mass percentages of TCA in the PDMS thin films. The reflection values decreased with increasing TCA concentration. This is consistent with previous work that showed reflection decreased as more gold was embedded throughout the polymer.[25] Switching the orientation of the thin film did not have a measurable effect on the measured transmission and reflection values. This was consistent with SEM and optical images in Figure 2 that indicate neither solid gold film nor large gold particles accumulate preferentially at the polymer film surface.

Introduction of the stainless steel support mesh led to an overall increase in attenuation for each film. This result is significant because the support mesh must be present to protect PDMS films against collapse into a permeate vacuum during operation of the plasmonic pervaporation system. The mesh increased reflectivity slightly, but reflection of each pair of thin film/support mesh was still relatively small. Transmission decreased substantially and in proportion to increasing $\log_{10}$ TCA concentration, corresponding to an overall increase in attenuation upon the addition of the reflective support mesh. The resulting attenuation values were 0.9501 ± 0.0231, 0.7854 ± 0.0107, 0.5052 ± 0.0149, and 0.4436 ± 0.0150 for the 0.5, 0.05, and 0.005 mass percent and PDMS respectively, as Figure 4 illustrates. The mesh used for this work is finer and has a more rigid structure than that used in previous work, leading to different reflective and transmissive properties.[25]

3.8. Thermal Properties. The magnitude of thermal response in the asymmetric thin films was higher than in three other methods for preparing thermoplasmonic nanocomposite media tested previously by our group. As summarized in Table 1, the thermal response in 0.05 mass percent AuNP-PDMS asymmetric film was 3× higher than previous measurements in AuNP-PDMS thin films in which AuNPs were uniformly distributed throughout the film prior to curing. The thermal response was 11× higher than when AuNPs were thermally transformed from electroless-plated Au thin film, and it was 230× higher than AuNPs suspended in aqueous solution. The 0.5 mass percent sample reached an average temperature in the laser spot 54.5°C above the ambient temperature of 23 °C, while the 0.05 mass percent, 0.005 mass percent, and Au-free PDMS samples reached 29.9 °C, 8.2 °C, and 0.7 °C above ambient, respectively. The laminar film had an average temperature change of 28.2 °C.

Temperature increased in each asymmetric film in linear proportion to attenuation both with and without the support mesh. Figure 5 shows the measured average temperature increase of each asymmetric film. Figure 6 displays the heat maps for each diffusive thin film after being allowed sufficient time to reach a steady-state temperature range. This increase in

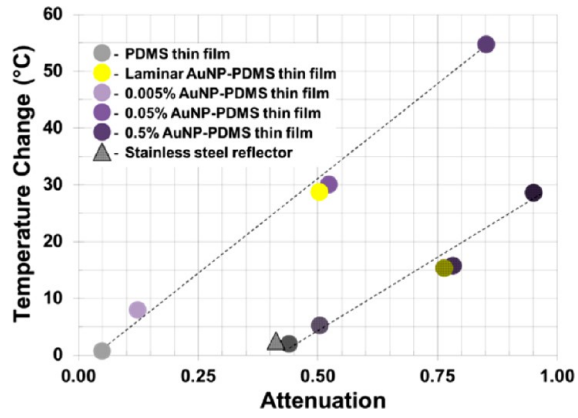

Figure 5. The relationships between attenuation and temperature change for the thin films with and without the stainless steel mesh. The triangle with cross-hatching (△) represents the support mesh. Circles with cross-hatching represent coupled data from each thin film of the corresponding color when paired with the reflector.

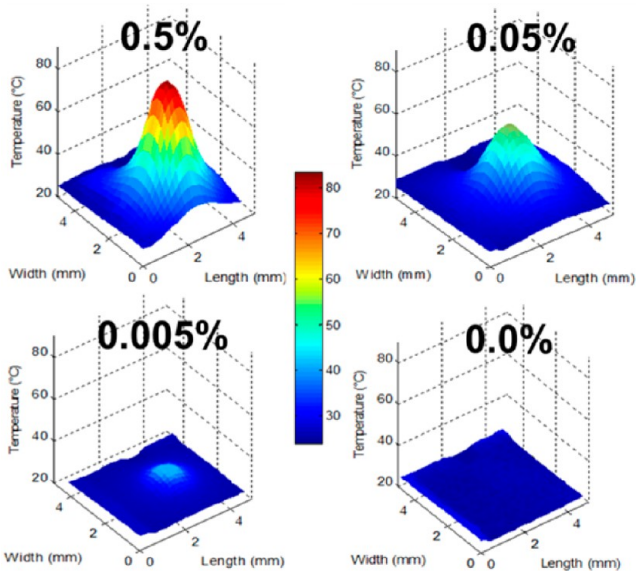

Figure 6. Temperature distributions for PDMS exposed to increasing concentrations of hydrogen tetrachloroaurate (TCA): 0.0 mass percent TCA (0.0%), 0.005 mass percent TCA (0.005%), 0.05 mass percent TCA (0.05%), and 0.5 mass percent TCA (0.5%) at 18 mW of incident irradiation.

thermal response relative to previous aqueous, silica, and PDMS samples appears to result from an increase in nanoparticle density relative to insulating PDMS, insulation of the heated layer by a thicker, adjacent gold-free PDMS, and reduction of radiativity of the PDMS relative to planar substrates. Preliminary modeling results indicate each of these three factors contribute significantly to the improvements over the previous work with uniformly distributed AuNPs.[22] These promising early results are the subject of an ongoing investigation.

Supporting the asymmetric Au-PDMS thin film with the stainless steel mesh reduced the thermoplasmonic temperature increase by about 50% in general. As Figure 5 shows, the 0.5 mass percent sample reached an average temperature in the laser spot 28.9°C above ambient, while the 0.05, 0.005, and PDMS samples reached 14.9°C and 5.0 °C, respectively. The laminar film reached an average of 14.8°C above ambient. The temperatures of the composite system appeared to follow the same linearity with attenuation as was demonstrated without the mesh; however, the overall temperature changes are considerably less. The support mesh acted as a radiator, conducting thermal energy away from plasmonically-heated AuNP-PDMS films into the surrounding environment. Incident irradiation of the mesh alone caused a temperature increase of 2.1 °C. The temperature change of the Au-free PDMS supported by the mesh was near this value (1.9 °C).

The parallel increases in attenuation and temperature suggest that photon-to-plasmon-to-heat transduction efficiency remains constant as Au content increases in the asymmetric AuNP-PDMS films. Modeling of the thermal behavior for comparison with previous work modeling thermal characteristics of isolated AuNPs in planar and uniform polymer geometries as well as in regular assemblies[38−40] is in progress. Reported studies also considered uniform molecular coating and local thermal properties.[41] These prior studies relate temperature distributions from uniform AuNP distributions to optical and physical properties of thermoplasmonic elements. The heterogeneous AuNP morphologies, asymmetric 3-D distribution, and multiple associated phases require further development of available models to correlate AuNPs properties in PDMS to kinetic and equilibrium thermoplasmonic temperature changes.

3.9. Evaluation for Use in Plasmonic Pervaporation. The scalability, heating capability, and asymmetry of these AuNP-PDMS films show significant potential in plasmonic heating applications, particularly in a plasmonic pervaporation system recently described.[27] Morphological, optical, and thermal characteristics distinguished in this work suggest that the AuNP-containing layer thickness can be reduced by factors of 10 or more relative to prior work, while providing improved thermoplasmonic heating. Efficient optoplasmonic conversion, providing localized heat, is an important aspect of the thin films as separation membranes.

The thermodynamic driving force in pervaporation is the difference in partial pressure between the feed and permeate sides of the membrane. Increasing the temperature at the permeate interface using asymmetric AuNP-PDMS thin film would increase this driving force. The asymmetry of the thin films is desirable because the effect of the AuNPs on the mass transport properties of PDMS remains largely uncharacterized. Placing the Au-free PDMS layer in contact with the pervaporation feed side and making the AuNP-PDMS layer as thin as possible should result in transport characteristics and performance of the thin films in membrane separation more analogous to Au-free PDMS, a commonly-used dense, hydrophobic membrane. A prior work illustrates pervaporation and mass transport across the membrane schematically in Figures 1 and 2.[42] The implementation of the films generated in this work to pervaporate liquids is ongoing and will be the subject of a future report.

Reduction of Au in partially cured PDMS via solution diffusion appeared superior to either reduction of Au in fully cured PDMS or laminar formation of asymmetric Au-PDMS thin films. A thinner Au layer was produced quickly with a wider range of attainable optical and physical properties and superior curability. The diffusive method produced AuNP-containing layers 3−7 times thinner than the laminar method, and further thickness reduction is anticipated by reducing exposure time or increasing pre-cure time. The possibility of further thickness reduction in the AuNP-containing layer with the diffusive method is intriguing since flux is inversely proportional to membrane thickness. Significant improvements to Au layer thickness and optothermal conversion are not anticipated for the laminar method. The practical limit to spin-coating PDMS appears to be about 10−15 μm, and this is possible only by using high concentrations of toluene which further complicate characterization of the thin films.[28] Significant optothermal efficiency improvements in the laminar method are not anticipated because the 1.2 mass percent TCA used in the AuNP-containing layer appears near the allowable limit for the PDMS to cure properly. Recently, an approach to obtain ordered arrays of layered sheets of ordered AuNP chains was presented.[43] While optical and thermal characteristics of the resulting nanocomposites were not quantified, this approach or a similar method could have significant potential in future work.

4. CONCLUSIONS

Reduction of aqueous hydrogen tetrachloroaurate (TCA) in a partially cured polydimethylsiloxane (PDMS) thin film rapidly formed an asymmetric film containing AuNPs only at the TCA-

exposed interface. Multi-scale morphological, optical, and thermoplasmonic characterization of resulting asymmetric films showed substantial benefits for heating applications such as plasmonic pervaporation. Reduction into a partially cured PDMS film via solution diffusion outperformed lamination of AuNP-containing films in terms of optothermal response, robustness, and scalability. Metallic nanoparticles, networks, and conglomerates were formed via reduction as the amount of dissolved TCA increased across a $\log_{10}$ scale. Increasing TCA concentrations caused polymer surface cratering, leading to a larger effective surface area. Both optical attenuation and thermoplasmonic temperature rise increased linearly with $\log_{10}$ increases in TCA content. In particular, the asymmetric AuNP-PDMS thin film formed from 0.5 mass percent TCA was 52-μm-thick with a 7 μm AuNP-containing layer, attenuated 0.85 of incident radiation, and produced an average temperature change of 54.5 °C at only 18 mW of incident resonant irradiation. The thermoplasmonic response of this asymmetric gold film was 3000 °C/watt, which was 3-, 11-, and 230-fold larger than comparable results using reduced TCA, annealed Au films, or suspended AuNP samples, respectively. Reduced thickness and improved heating capacity in asymmetric Au-PDMS thin films obtained by reduction of TCA that is diffusing in partially cured polymer could lead to a substantial increase in solvent flux during pervaporation.

AUTHOR INFORMATION

Corresponding Author

*Phone: (479) 575-6691. Fax: (479) 575-7926. E-mail: dkroper@uark.edu.

Author Contributions

J.R.D. and G.T.F. performed experiments, analyzed data, and prepared text and figures for the manuscript. D.K.R. directed the work and organized the final text.

Notes

The authors declare no competing financial interest.

ACKNOWLEDGMENTS

This work was supported in part by NSF CMMI-0909749, NSF CBET-1134222, NSF ECCS-1006927, the University of Arkansas Foundation, and the Walton Family Charitable Foundation. Any opinions, findings, and conclusions or recommendations expressed in this material are those of the authors and do not necessarily reflect the views of the National Science Foundation. The authors would like to thank D. DeJarnette for SEM imaging and P. Blake for helpful discussions. The authors greatly appreciate the use of the Arkansas Materials Characterization Facility and are grateful to M. Benamara for the TEM analysis.

ABBREVIATIONS

Au, gold; AuNP, gold nanoparticle; PDMS, polydimethylsiloxane; TCA, hydrogen tetrachloroaurate; LSPR, localized surface plasmon resonance; η, cross-linker to monomer ratio

REFERENCES

(1) Tong, S. W.; Zhang, C. F.; Jiang, C. Y.; Liu, G.; Ling, Q. D.; Kang, E. T.; Chan, D. S. H.; Zhu, C. *Chem. Phys. Lett.* **2008**, *453*, 73−76.

(2) Wang, C. C. D.; Choy, W. C. H.; Duan, C.; Fung, D. D. S.; Sha, W. E. I.; Xie, F.-X.; Huang, F.; Cao, Y. *J. Mater. Chem.* **2012**, *22*, 1206−1211.

(3) Xie, F.-X.; Choy, W. C. H.; Wang, C. C. D.; Sha, W. E. I.; Fung, D. D. S. *Appl. Phys. Lett.* **2011**, *99*, 153304−1-153304-3.

(4) Akimov, Y. A; Koh, W. S.; Ostrikov, K. *Opt. Express* **2009**, *17*, 10195−101205.

(5) Ofir, Y.; Samanta, B.; Rotello, V. M. *Chem. Soc. Rev.* **2008**, *37*, 1814−1825.

(6) Nergiz, S. Z.; Singamaneni, S. *ACS Appl. Mater. Interfaces* **2011**, *3*, 945−951.

(7) Massaro, A.; Spano, F.; Cingolani, R.; Athanassiou, A. *IEEE Sens. J.* **2011**, *11*, 1780−1786.

(8) Matsui, J.; Akamatsu, K.; Nishiguchi, S.; Miyoshi, D.; Nawafune, H.; Tamaki, K.; Sugimoto, N. *Anal. Chem.* **2004**, *76*, 1310−1315.

(9) Zamborini, F. P.; Leopold, M. C.; Hicks, J. F.; Kulesza, P. J.; Malik, M. A; Murray, R. W. *J. Am. Chem. Soc.* **2002**, *124*, 8958−8964.

(10) Monson, T. C.; Hollars, C. W.; Orme, C. A.; Huser, T. *ACS Appl. Mater. Interfaces* **2011**, *3*, 1077−1082.

(11) Shi, J.; Chan-Park, M. B.; Li, C. M. *ACS Appl. Mater. Interfaces* **2011**, *3*, 1880−1886.

(12) Ko, S. H.; Pan, H.; Grigoropoulos, C. P.; Luscombe, C. K.; Fréchet, J. M. J.; Poulikakos, D. *Nanotechnology* **2007**, *18*, 345202 (8pp).

(13) Noh, Y.-Y.; Zhao, N.; Caironi, M.; Sirringhaus, H. *Nat. Nanotechnol.* **2007**, *2*, 784−789.

(14) Tseng, R. J.; Huang, J.; Ouyang, J.; Kaner, R. B.; Yang, Y. *Nano Lett.* **2005**, *5*, 1077−1080.

(15) Ouyang, J.; Chu, C.-W.; Szmanda, C. R.; Ma, L.; Yang, Y. *Nat. Mater.* **2004**, *3*, 918−922.

(16) Shenhar, R.; Norsten, T. B.; Rotello, V. M. *Adv. Mater.* **2005**, *17*, 657−669.

(17) Yang, H.; Nagai, K.; Abe, T.; Homma, H.; Norimatsu, T.; Ramaraj, R. *ACS Appl. Mater. Interfaces* **2009**, *1*, 1860−1864.

(18) Vanherck, K.; Hermans, S.; Verbiest, T.; Vankelecom, I. *J. Mater. Chem.* **2011**, *21*, 6079−6087.

(19) Scott, A.; Gupta, R.; Kulkarni, G. U. *Macromol. Chem. Phys.* **2010**, *211*, 1640−1647.

(20) Ryu, D.; Loh, K. J.; Ireland, R.; Karimzada, M.; Yaghmaie, F.; Gusman, A. M. *Smart Struct. Syst.* **2011**, *8*, 471−486.

(21) Goyal, A.; Kumar, A.; Patra, P. K.; Mahendra, S.; Tabatabaei, S.; Alvarez, P. J. J.; John, G.; Ajayan, P. M. *Macromol. Rapid Commun.* **2009**, *30*, 1116−1122.

(22) Berry, K. R.; Russell, A. G.; Blake, P. A.; Roper, D. K. *Nanotechnology* **2012**, *23*, 375703 (11pp).

(23) Zhang, Q.; Xu, J.-J.; Liu, Y.; Chen, H.-Y. *Lab Chip* **2008**, *8*, 352−357.

(24) Kaur, J.; Lee, J. H.; Bucknall, D. G.; Shofner, M. L. *ACS Appl. Mater. Interfaces* **2012**, *4*, 3111−3121.

(25) Forcherio, G. T.; Roper, D. K. *Appl. Opt.* **2013**, Accepted.

(26) Simpson, T. R. E.; Tabatabaian, Z.; Jeynes, C.; Parbhoo, B.; Keddie, J. L.; Al, S. E. T. *J. Polym. Sci., Part A: Polym. Chem. A* **2004**, *42*, 1421−1431.

(27) Russell, A. *Plasmonic Pervaporation via Gold Nanoparticle-Functionalized Nanocomposite Membranes*, Ph.D. Thesis, University of Arkansas, 2012.

(28) Park, J.; Kim, H. S.; Han, A. *J. Micromech. Microeng.* **2009**, *19*, 65016.

(29) Bastús, N. G.; Comenge, J.; Puntes, V. *Langmuir* **2011**, *27*, 11098−11105.

(30) Harada, M.; Tamura, N.; Takenaka, M. *J. Phys. Chem. C* **2011**, *115*, 14081−14092.

(31) Patil, S. A.; Shinde, D. V.; Kim, E.; Lee, J. K.; Mane, R. S.; Han, S.-H. *RSC Adv.* **2012**, *2*, 11808−11812.

(32) Watson, J. M.; Baron, M. G. *J. Membr. Sci.* **1995**, *106*, 259−268.

(33) Harada, M.; Okamoto, K.; Terazima, M. *J. Colloid Interface Sci.* **2009**, *332*, 373−381.

(34) Russell, A. G.; McKnight, M. D.; Hestekin, J. A; Roper, D. K. *Langmuir* **2011**, *27*, 7799−7805.

(35) Russell, A. G.; McKnight, M. D.; Sharp, A. C.; Hestekin, J. A.; Roper, D. K. *J. Phys. Chem. C* **2010**, *114*, 10132−10139.

(36) Ahn, W.; Roper, D. K. *J. Phys. Chem. C* **2008**, *112*, 12214−12218.
(37) Roper, D. K.; Ahn, W.; Hoepfner, M. *J. Phys. Chem. C* **2007**, *111*, 3636−3641.
(38) Baffou, G.; Quidant, R.; García de Abajo, F. J. *ACS Nano* **2010**, *4*, 709−716.
(39) Rodriques-Oliveros, R.; Sanchez-Gil, J. *Opt. Express* **2012**, *20*, 402−407.
(40) Baffou, G.; Quidant, R. *Laser Photonics Rev.* **2012**, *17*, 1−17.
(41) Baffou, G.; Quidant, R.; Girard, C. *Phys. Rev. B: Condens. Matter Mater. Phys.* **2010**, *82*, 1−11.
(42) Satyanarayana, S. V.; Sharma, A.; Bhattacharya, P. K. *Chem. Eng. J.* **2004**, *102*, 171−184.
(43) Kao, J.; Bai, P.; Chuang, V. P.; Jiang, Z.; Ercius, P.; Xu, T. *Nano Lett.* **2012**, *12*, 2610−2618.